Design and optical characterization of high-Q guided-resonance modes in the slot-graphite photonic crystal lattice

Luis Javier Martínez,* Ningfeng Huang, Jing Ma, Chenxi Lin, Eric Jaquay, and Michelle L. Povinelli

Ming Hsieh Department of Electrical Engineering, University of Southern California, Powell Hall of Engineering, 3737 Watt Way, Los Angeles, CA 90089-0271, USA

*ljmartin@usc.edu

http://www.usc.edu/nanophotonics

Abstract: A new photonic crystal structure is generated by using a regular graphite lattice as the base and adding a slot in the center of each unit cell to enhance field confinement. The theoretical Q factor in an ideal structure is over 4×10^5. The structure was fabricated on a silicon-on-insulator wafer and optically characterized by transmission spectroscopy. The resonance wavelength and quality factor were measured as a function of slot height. The measured trends show good agreement with simulation.

OCIS codes: (220.0220) Optical design and fabrication; (230.5298) Photonic crystals; (350.4855) Optical tweezers or optical manipulation.

References and links

1. S. Noda and T. Baba, *Roadmap on Photonic Crystals* (Kluwer Academic Publisher, 2003), 1st ed.
2. S. Noda, "Recent progresses and future prospects of two- and three-dimensional photonic crystals," J. Lightw. Technol. **24**, 4554–4567 (2006).
3. T. Ochiai and K. Sakoda, "Dispersion relation and optical transmittance of a hexagonal photonic crystal slab," Phys. Rev. B **63**, 125107 (2001).
4. M. Zelsmann, E. Picard, T. Charvolin, E. Hadji, M. Heitzmann, B. Dal'zotto, M. E. Nier, C. Seassal, P. Rojo-Romeo, and X. Letartre, "Seventy-fold enhancement of light extraction from a defectless photonic crystal made on silicon-on-insulator," Appl. Phys. Lett. **83**, 2542–2544 (2003).
5. H.-Y. Ryu, S.-H. Kwon, Y.-J. Lee, Y.-H. Lee, and J.-S. Kim, "Very-low-threshold photonic band-edge lasers from free-standing triangular photonic crystal slabs," Appl. Phys. Lett. **80**, 3476–3478 (2002).
6. J. Mouette, C. Seassal, X. Letartre, P. Rojo-Romeo, J.-L. Leclereq, P. Regreny, P. Viktorovitch, E. Jalaguier, R. Perreau, and H. Moriceau, "Very low threshold vertical emitting laser operation in InP graphite photonic crystal slab on silicon," Electron. Lett. **39**, 526–528 (2003).
7. M. Notomi, H. Suzuki, and T. Tamamura, "Directional lasing oscillation of two-dimensional organic photonic crystal lasers at several photonic band gaps," Appl. Phys. Lett. **78**, 1325–1327 (2001).
8. L. J. Martínez, B. Alén, I. Prieto, J. F. Galisteo-López, M. Galli, L. C. Andreani, C. Seassal, P. Viktorovitch, and P. A. Postigo, "Two-dimensional surface emitting photonic crystal laser with hybrid triangular-graphite structure," Opt. Express **17**, 15043–15051 (2009).
9. F. Raineri, G. Vecchi, A. M. Yacomotti, C. Seassal, P. Viktorovitch, R. Raj, and A. Levenson, "Doubly resonant photonic crystal for efficient laser operation: Pumping and lasing at low group velocity photonic modes," Appl. Phys. Lett. **86**, 011116 (2005).
10. B. Zhen, S.-L. Chua, J. Lee, A. W. Rodriguez, X. Liang, S. G. Johnson, J. D. Joannopoulos, M. Soljačić, and O. Shapira, "Enabling enhanced emission and low-threshold lasing of organic molecules using special Fano resonances of macroscopic photonic crystals," Proc. Natl. Acad. Sci. **110**, 13711–13716 (2013).
11. M. Huang, A. A. Yanik, T.-Y. Chang, and H. Altug, "Sub-wavelength nanofluidics in photonic crystal sensors," Opt. Express **17**, 24224–24233 (2009).

#198966 - $15.00 USD Received 7 Oct 2013; revised 10 Nov 2013; accepted 18 Nov 2013; published 9 Dec 2013

12. M. E. Beheiry, V. Liu, S. Fan, and O. Levi, "Sensitivity enhancement in photonic crystal slab biosensors," Opt. Express **18**, 22702–22714 (2010).
13. L. C. Estrada, O. E. Martinez, M. Brunstein, S. Bouchoule, L. Le-Gratiet, A. Talneau, I. Sagnes, P. Monnier, J. A. Levenson, and A. M. Yacomotti, "Small volume excitation and enhancement of dye fluorescence on a 2D photonic crystal surface," Opt. Express **18**, 3693–3699 (2010).
14. T. Kaji, T. Yamada, R. Ueda, and A. Otomo, "Enhanced fluorescence emission from single molecules on a two-dimensional photonic crystal slab with low background emission," J. Phys. Chem. Lett. **2**, 1651–1656 (2011).
15. N. Ganesh, W. Zhang, P. C. Mathias, E. Chow, J. Soares, V. Malyarchuk, A. D. Smith, and B. T. Cunningham, "Enhanced fluorescence emission from quantum dots on a photonic crystal surface," Nat Nanotechnology **2**, 515 – 520 (2007).
16. C. A. Mejia, A. Dutt, and M. L. Povinelli, "Light-assisted templated self assembly using photonic crystal slabs," Opt. Express **19**, 11422–11428 (2011).
17. E. Jaquay, L. J. Martínez, C. A. Mejia, and M. L. Povinelli, "Light-assisted, templated self-assembly using a photonic-crystal slab," Nano Letters **13**, 2290–2294 (2013).
18. J. Ma, L. J. Martínez, and M. L. Povinelli, "Optical trapping via guided resonance modes in a slot-Suzuki-phase photonic crystal lattice," Opt. Express **20**, 6816–6824 (2012).
19. V. R. Almeida, Q. Xu, C. A. Barrios, and M. Lipson, "Guiding and confining light in void nanostructure," Opt. Lett. **29**, 1209–1211 (2004).
20. X. Letartre, J. Mouette, J. Leclercq, P. Rojo Romeo, C. Seassal, and P. Viktorovitch, "Switching devices with spatial and spectral resolution combining photonic crystal and MOEMS structures," J. Lightw. Technol. **21**, 1691 – 1699 (2003).
21. X. Letartre, C. Monat, C. Seassal, and P. Viktorovitch, "Analytical modeling and an experimental investigation of two-dimensional photonic crystal microlasers: defect state (microcavity) versus band-edge state (distributed feedback) structures," J. Opt. Soc. Am. B **22**, 2581–2595 (2005).
22. L. Ferrier, P. Rojo-Romeo, E. Drouard, X. Letatre, and P. Viktorovitch, "Slow bloch mode confinement in 2D photonic crystals for surface operating devices," Opt. Express **16**, 3136–3145 (2008).
23. H. Akhavan, M. El-Beheiry, R. Schilling, D. Aydin, and O. Levi, "Evaluation of high quality factor photonic crystal slabs for biosensing," in "CLEO:2011 - Laser Applications to Photonic Applications," (Optical Society of America, 2011), p. JWA105.
24. G. Alagappan, X. W. Sun, and H. D. Sun, "Symmetries of the eigenstates in an anisotropic photonic crystal," Phys. Rev. B **77**, 195117 (2008).
25. L. C. Andreani and D. Gerace, "Photonic-crystal slabs with a triangular lattice of triangular holes investigated using a guided-mode expansion method," Phys. Rev. B **73**, 235114 (2006).
26. K. Sakoda, *Optical Properties of Photonic Crystals* (Springer-Verlag, Berlin, 2004), 2nd ed.
27. T. Yamamoto, M. Notomi, H. Taniyama, E. Kuramochi, Y. Yoshikawa, Y. Torii, and T. Kuga, "Design of a high-*Q* air-slot cavity based on a width-modulated line-defect in a photonic crystal slab," Opt. Express **16**, 13809–13817 (2008).
28. C. Lin, L. J. Martínez, and M. L. Povinelli, "Fabrication of transferrable, fully suspended silicon photonic crystal nanomembranes exhibiting vivid structural color and high-*Q* guided resonance," J. Vac. Tech. B **31**, 050606 (2013).
29. M. Skorobogatiy, G. Bégin, and A. Talneau, "Statistical analysis of geometrical imperfections from the images of 2D photonic crystals," Opt. Express **13**, 2487–2502 (2005).
30. V. Astratov, M. Skolnick, S. Brand, T. Krauss, O. Z. Karimov, R. M. Stevenson, D. Whittaker, I. Culshaw, and R. De La Rue, "Experimental technique to determine the band structure of two-dimensional photonic lattices," Optoelectronics, IEE Proceedings - **145**, 398–402 (1998).
31. V. N. Astratov, D. M. Whittaker, I. S. Culshaw, R. M. Stevenson, M. S. Skolnick, T. F. Krauss, and R. M. De La Rue, "Photonic band-structure effects in the reflectivity of periodically patterned waveguides," Phys. Rev. B **60**, R16255–R16258 (1999).
32. Y. Nazirizadeh, U. Bog, S. Sekula, T. Mappes, U. Lemmer, and M. Gerken, "Low-cost label-free biosensors using photonic crystals embedded between crossed polarizers," Opt. Express **18**, 19120–19128 (2010).
33. N. Huang, L. J. Martínez, and M. L. Povinelli, "Tuning the transmission lineshape of a photonic crystal slab guided-resonance mode by polarization control," Opt. Express **21**, 20675–20682 (2013).
34. D. L. C. Chan, I. Celanovic, J. D. Joannopoulos, and M. Soljačić, "Emulating one-dimensional resonant *Q*-matching behavior in a two-dimensional system via Fano resonances," Phys. Rev. A **74**, 064901 (2006).

1. Introduction

Since the first studies of two-dimensional (2D) photonic crystal slabs [1], these structures have attracted considerable interest [2]. One particularly interesting feature of photonic-crystal slabs is that they support guided-resonance modes at the Γ point, corresponding to zero in-plane wave vector [3]. Γ-point modes with the appropriate symmetry properties are excited by nor-

#198966 - $15.00 USD Received 7 Oct 2013; revised 10 Nov 2013; accepted 18 Nov 2013; published 9 Dec 2013

mally incident light, giving rise to a standing Bloch wave within the slab. Γ-point modes have been used for a variety of applications, including extraction of light from semiconductors [4], lasing [5-10], and sensing [11, 12]. They have also been used for enhancement of fluorescence in dyes [10, 13], single molecules [14], and colloidal quantum dots [15]. We have proposed [16] and demonstrated [17] the use of Γ-point modes for large-area optical trapping of nanoparticles in regular arrays, a process we call light-assisted, templated self assembly (LATS). To minimize the optical power required for LATS, it is advantageous to use a mode for which the field intensity is strongly concentrated at each optical trapping site [18]. In this work, we design, fabricate and characterize a novel photonic-crystal lattice that supports a Γ-point mode with both strong spatial field concentration and high, tunable quality factor.

The novel photonic-crystal lattice we demonstrate is based on the principle of slot enhancement [19]. Due to the boundary conditions on the electric field, a narrow slot in a dielectric will strongly enhance the electric field perpendicular to the slot, and hence the local electromagnetic field intensity. This effect was initially studied in on-chip waveguides, where light propagates along the length of the slot [19]. In a previous theoretical paper [18], we showed that slot enhancement can also be used to create localized, high-intensity regions within an extended area guided-resonance mode. In this case, the mode couples to light propagating at normal incidence to the slots. Our initial design was based on a Suzuki-phase lattice. For the experimental demonstration shown here, we chose a graphite lattice as basis. By introducing a slot into each unit cell of the original lattice, we create a mode with strong electromagnetic field confinement within each slot. By tuning the slot dimensions, we obtain a theoretical quality factor (Q) larger than 10^5. In comparison to our previous design, our *slot-graphite lattice* has a flatter band at the Γ point, a property known to correlate with high experimental values of Q in finite-size structures [20-22]. We fabricated our slot-graphite lattice in a silicon-on-insulator platform and characterized the structure via optical transmission spectroscopy. We obtained experimental Q values as high as 5000 for samples measured in water, comparable to state-of-the-art values in the literature [23]. We further demonstrated experimental tuning of the resonant wavelength and Q factor with slot dimension and found that the trends are well predicted by simulation. We expect that our high-Q, Γ-point slot mode will be useful for LATS, as well as for other photonic-crystal slab applications.

2. Structure design

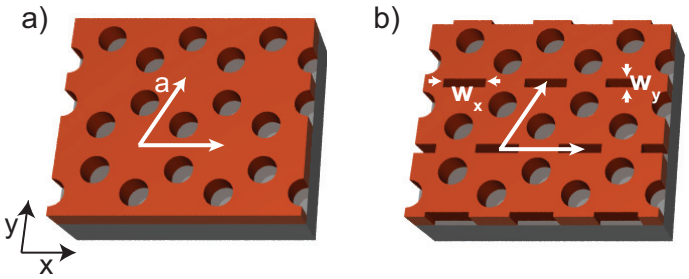

Fig. 1. a) Diagram of the graphite photonic crystal lattice. b) Diagram of the slot-graphite photonic crystal lattice. The arrows represent the primitive vectors of the Bravais lattice.

We create the slot-graphite lattice by introducing a rectangular slot with dimensions $w_x \times w_y$ in the center of each unit cell of the graphite lattice, as shown in Fig. 1. The slot-graphite lattice has the same Bravais lattice as the original graphite lattice. However, the slot reduces the lattice symmetry from C_{6v} to C_{2v} [24]. The reduced symmetry increases the size of the

#198966 - $15.00 USD Received 7 Oct 2013; revised 10 Nov 2013; accepted 18 Nov 2013; published 9 Dec 2013

irreducible Brillouin zone. The irreducible Brillouin zone of the graphite lattice is shown in the inset to Fig. 2(a) and is 1/12 of the first Brillouin zone. We label it by Γ-M-K-Γ. The irreducible Brillouin zone of the slot-graphite lattice is shown in the inset to Fig. 2(b) and is 1/4 of the first Brillouin zone. We label it Γ-M-K-M1-K1-Γ.

Figure 2(a) shows the 3D photonic band structure of the graphite lattice. The bands are calculated using a guided-mode expansion method [25]. We assume a lattice constant $a = 800$ nm, a hole radius $r = 0.157a$, and a slab thickness of 250 nm lying on top of a silica layer and immersed in a material of dielectric constant $\varepsilon_b = 1.77$. The bands are the same along the M-Γ-K boundary and the M1-Γ-K1 boundary. At the Γ point, as highlighted by dashed ellipses, the fourth and fifth bands are degenerate. The corresponding mode profiles are shown in Fig. 2(c). The H_z components of the two degenerate modes have dipole-like field distributions with different orientations, and thus we refer to them as dipole modes. From group theory, the point group at the Γ point is the symmetry group of the lattice. C_{6v} supports two two-dimensional irreducible representations and two one-dimensional irreducible representations. The dipole modes shown in Fig. 2(c) belong to the E_1 irreducible representation [26], which allows coupling to an incident plane wave. The fourth and fifth modes couple to incident *x*- and *y*- polarized light, respectively.

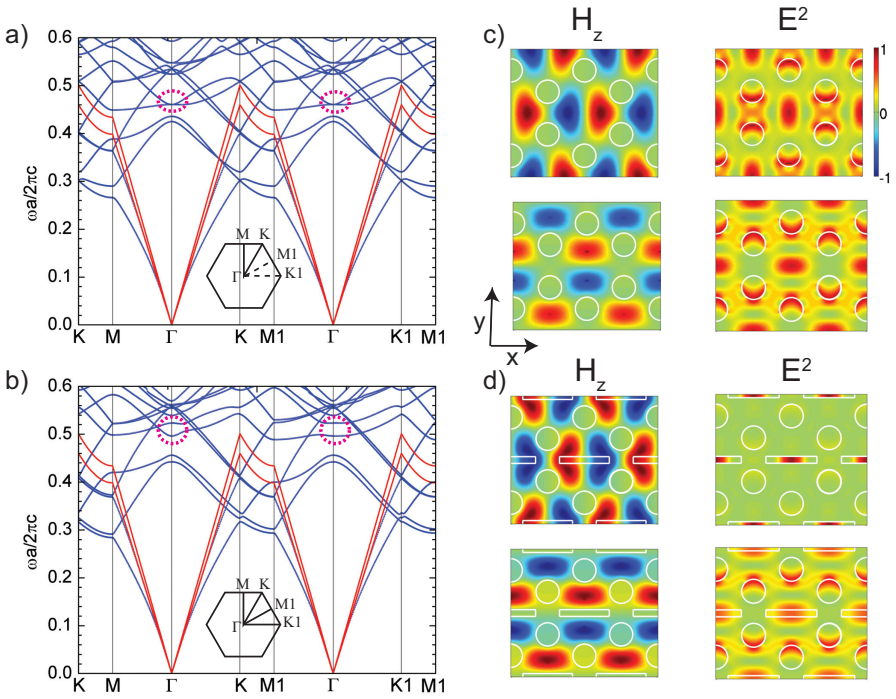

Fig. 2. a) Photonic band structure of the graphite photonic crystal lattice. b) Photonic band structure of the slot-graphite photonic crystal lattice. Upper red line represents the light line of the upper cladding material. Bottom red line represents silica light line. c) H_z-field profile (left) and E^2 profile (right) of the fourth band (above) and fifth band (below) of the graphite photonic crystal lattice. d) H_z-field profile (left) and E^2 profile (right) of the fourth band (below) and fifth band (above) of the slot-graphite photonic crystal lattice.

Figure 2(b) shows the band structure of our slot-graphite lattice. The slot dimensions are

#198966 - $15.00 USD Received 7 Oct 2013; revised 10 Nov 2013; accepted 18 Nov 2013; published 9 Dec 2013

$w_x = 0.675a$ and $w_y = 0.09a$. The other geometrical parameters are identical with the graphite lattice. The bands along the M-Γ-K boundary and the M1-Γ-K1 boundary are different, as can easily be seen by comparing the dashed ellipses. At the Γ point, the degeneracy of the fourth and fifth bands in the graphite lattice is removed due to introduction of the slot. For the slot-graphite lattice, the point group at the Γ point is reduced to C_{2v}. As a result, the two-dimensional E_1 irreducible representation of the C_{6v} group is split into two one-dimensional irreducible representations of the C_{2v} group (B_1 and B_2), which correspond to the fourth and fifth bands, respectively. Both bands couple to an incident plane wave. From the continuity conditions on the fields, the components of the displacement field $\vec{D} = \varepsilon\vec{E}$ perpendicular to the slot are continuous [19, 27]. This has the effect of concentrating E^2 for the *y*-polarized mode (the fifth band) within the slot region, as shown in Fig. 2(d) (upper row). We call this mode the *slot mode*. Light confinement within the slot is not apparent for the fourth band, which is polarized along the *x*-direction (Fig. 2(d), lower row). We refer to this mode as the *dipole mode*.

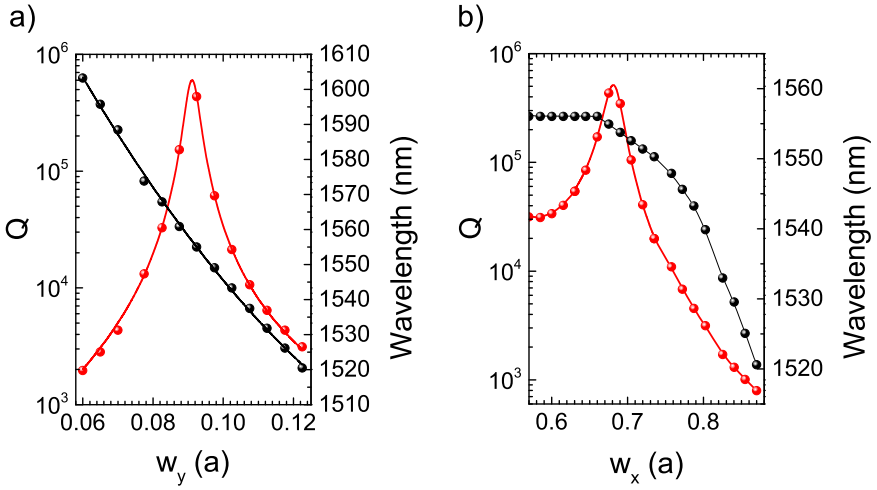

Fig. 3. a) Evolution of the simulated Q factor (red) and wavelength (black) as function a of w_y. b) Evolution of the simulated Q factor (red) and wavelength (black) as a function of w_x. Symbols indicate calculated values, and lines are guides to the eye.

We calculated the Q factor of the slot mode at the Γ point using the FDTD method (Lumerical). In Fig. 3(a), we vary the slot height w_y for a fixed slot width $w_x = 0.675a$. The Q factor is shown in red, and the wavelength is shown in black. A maximum value of $Q = 4.3 \times 10^5$ is obtained for $w_y = 0.0925a$. In Fig. 3(b), we fix w_y to the optimal value and vary w_x. We observe that Q is less affected by variations in w_x than w_y. For example, a change of 20 nm in w_x preserves a Q-factor over 85000 (20% of the peak value), while a change of 20 nm in w_y decreases Q from 4.3×10^5 to 4300 (1% of the initial value).

We evaluate the spatial field enhancement by considering the maximum electric field value for the slot mode. Given the same energy in the mode, this value is 3 times bigger than in the dipole mode of the graphite lattice. Given the same incident power, the maximum electric field value is 176 times larger than for the dipole mode of the graphite lattice, and 1513 times larger than for free space. This increase is due to the high Q factor of the mode, in addition to the spatial field enhancement. It is important to note that, for optimized slot dimensions, in comparison to our previous theoretical work on the slot Suzuki-phase lattice [18], the slot mode band is three times flatter at the Γ point; bands with smaller slope have the favourable effect of

#198966 - $15.00 USD Received 7 Oct 2013; revised 10 Nov 2013; accepted 18 Nov 2013; published 9 Dec 2013

increasing the lateral confinement in finite-sized structures [20-22].

3. Fabrication and optical characterization

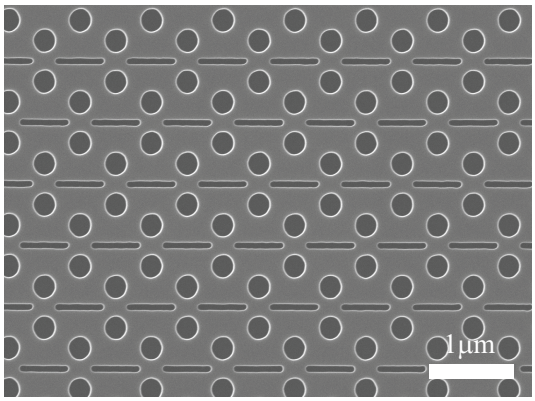

Fig. 4. SEM image of a fabricated slot-graphite device. The smallest slot dimension is $w_y = 59$ nm. See parameters in the main text.

We fabricated a group of slot-graphite photonic crystal devices in order to characterize the evolution of the slot modes with varying slot height w_y . The devices are fabricated with a fixed lattice constant of $a = 820$ nm, air hole radius $r/a = 0.155$, and slab thickness $t = 250$ nm.

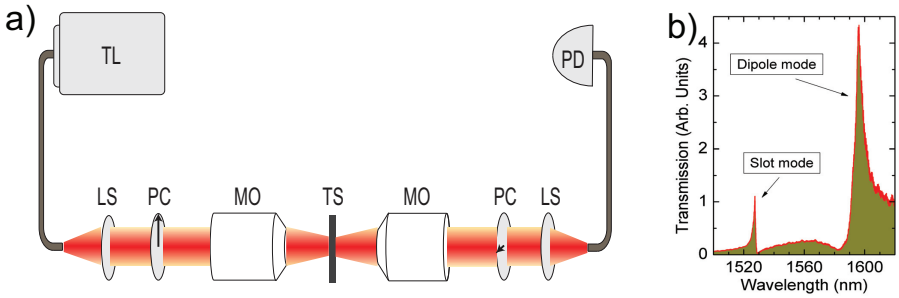

Fig. 5. a) Diagram of experimental setup used to characterize the optical properties of the photonic crystal lattices. Two crossed polarizers (PC) are applied before and after the device to cancel out Fabry-Pérot effects. TL: tunable laser; MO: microscope objective; LS: lens; TS: translation stage; PD: photodiode. b) A typical measured spectrum. The right transmission peak corresponds to the dipole mode, and the left peak corresponds to the slot mode, which has a higher Q factor.

The devices were fabricated using e-beam lithography and inductively-coupled plasma reactive ion etching (ICP-RIE). We used a 250 nm thick silicon layer on top of a 3 μm silica layer (SOITEC). The sample was spin-coated with PMMA-A4 950K. Using a Raith 150 e-beam system, a 50 μm diameter slot-graphite pattern was exposed with an acceleration voltage of 30 kV. The pattern was transferred from the resist to the silicon layer by ICP-RIE etching using a gas mixture of SF_6 and C_4F_8. Finally, the remaining resist was removed using O_2 plasma etching and acetone. Further details about the fabrication process can be found in Ref. [28]. Figure 4 shows a scanning electron micrograph (SEM) image of one of the fabricated devices. We analyzed the SEM images and extracted geometrical parameters [29]. The slot width w_x was fixed

#198966 - $15.00 USD Received 7 Oct 2013; revised 10 Nov 2013; accepted 18 Nov 2013; published 9 Dec 2013

to $\simeq$ 550 nm, and w_y was increased gradually from 59 nm to 95 nm by an average step of $\simeq$ 3.3 nm.

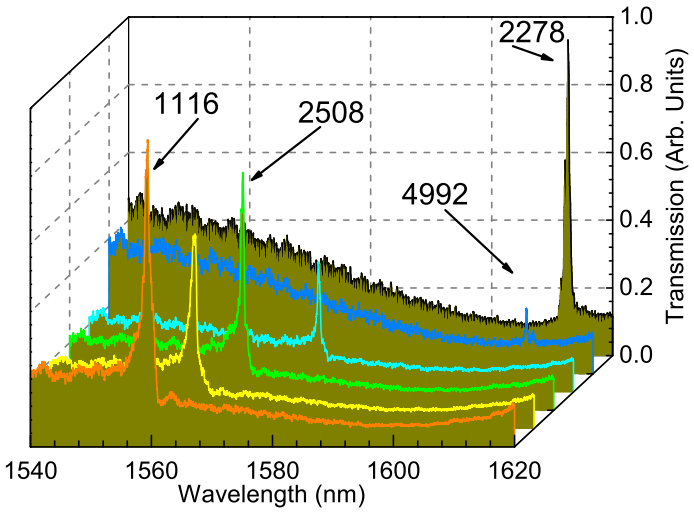

Fig. 6. Several representative spectra of the slot-graphite devices as the dimension w_y increases from $w_y \simeq 59$ nm (black curve) to $w_y \simeq 93$ nm (orange curve). The intermediate values are ∼62 nm, ∼80 nm, ∼83 nm and ∼87 nm. The other dimensions of the devices are kept constant. Numbers with arrows indicate Q factors.

We characterized the transmission spectra of our fabricated samples by means of the surface coupling technique at normal incidence [30, 31] using the experimental configuration shown in Fig. 5(a). The sample is immersed in deionized water. Incident light from a tunable laser (TL) in the near-infrared range between 1500 nm and 1620 nm is collimated from a fiber to free space by a lens (LS). The light is passed through a polarizer (PC) and focused by a low numerical aperture microscope objective (MO) onto the sample, which is mounted on a translation stage (TS). The light transmitted through the sample is collected using another microscope objective, passed through a second polarizer oriented perpendicular to the first, and coupled via a lens to a fiber-coupled photodetector (PD). The polarization angle of the incident light is 45° with respect to the longitudinal direction of the slot. With the crossed polarization setup, guided resonance modes appear as peaks in the transmission spectrum, rather than dips on a Fabry-Pérot background [32, 33]. A typical spectrum is shown in Fig. 5(b). We observe a narrower (higher Q factor) slot mode at lower wavelength and a wider (lower Q factor) dipole mode at higher wavelength.

Figure 6 shows representative spectra for several different values of the slot height w_y . This dimension increases from the smallest value of $w_y \simeq 59$ nm (black curve) to the largest value of $w_y \simeq 93$ nm (orange curve). The resonant peak shifts to lower wavelengths as the dimension of the slot increases. We fit the experimental spectra to a Fano function to accurately determine the resonant wavelength and Q factor [33]. Q factors for several devices are labeled with arrows in Fig. 6.

Figure 7(a) shows the dependence of the Q factor on slot height. The blue spheres are measured values, and the red line is a guide to the eye. We observe that the measured Q factor first increases and then decreases with increasing w_y. The highest measured value shown is ∼5000. This value is comparable to state-of-the-art values in the literature for coupled modes

#198966 - $15.00 USD Received 7 Oct 2013; revised 10 Nov 2013; accepted 18 Nov 2013; published 9 Dec 2013

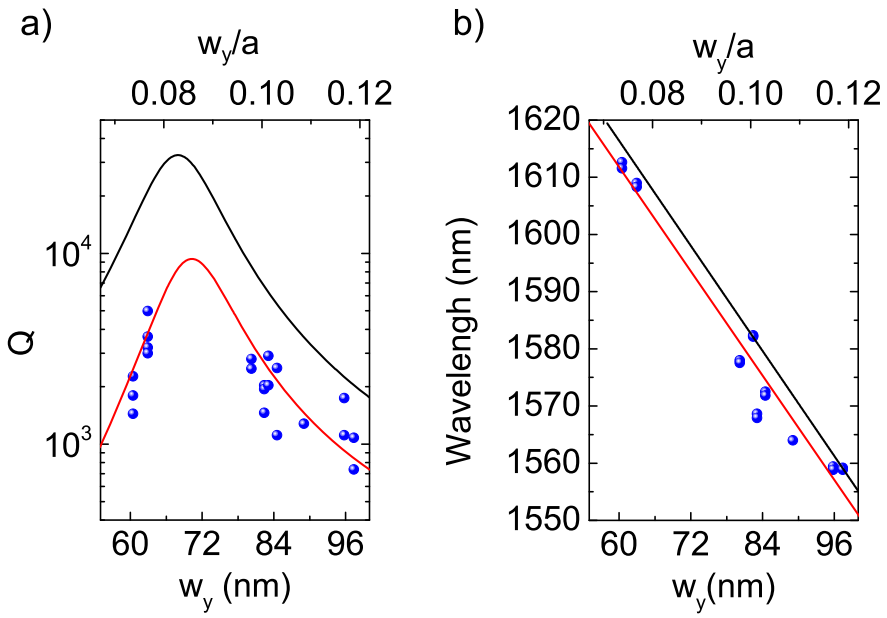

Fig. 7. a) Evolution of the Q factor as a function of w_y. b) Evolution of the wavelength as a function w_y. Blue dots represent experimental data. Black line represent simulated data. Red lines represent a guide to the eye in a) and a linear fit in b).

measured in water [23]. For devices with w_y between 68 nm and 78 nm, we obtained higher Q values (narrower spectral linewidths). However, since experimental noise prevented accurate measurement, the data is not shown. The black line shows calculated values from simulations. The simulation includes the effect of water absorption. The experimental Q values are lower than the simulated ones, which should be expected due to fabrication imperfection and surface roughness. Overall, the measured and simulated results show the same trend in Q with slot dimension.

Figure 7(b) shows the evolution of resonant wavelength with slot height. Blue spheres show measured values, the red line shows a linear fit, and the black line shows simulation results. The measured wavelength decreases monotonically from 1613 nm to 1560 nm as w_y increases from 59 nm to 95 nm. In this domain of values of w_y the evolution of wavelength with w_y can be approximated by a linear function (for values smaller than 60 nm the trend is not linear). From the fit, we observe that the experimental and simulation results show very good agreement (slope difference below 1% and vertical separation $\sim$5 nm).

4. Conclusions

We have proposed a new photonic-crystal slab structure, the slot-graphite lattice. It is created by placing a slot in the center of each unit cell of the graphite lattice. Simulations show that a mode is created with high electromagnetic field confinement in the slots. The theoretical Q value is higher than 10^5. We fabricated the structure on an SOI platform and characterized the mode via crossed-polarization transmission measurements. Q factor values up to 5000 have been measured, and the trends in Q and wavelength with slot height agree well with simulations.

Our new structure, which provides both a large, tunable Q factor and strong confinement near the slab surface, holds strong promise for light-assisted templated self assembly (LATS),

#198966 - $15.00 USD Received 7 Oct 2013; revised 10 Nov 2013; accepted 18 Nov 2013; published 9 Dec 2013

as well as for other applications of Γ-point modes in photonic-crystal slabs. For example, the ability to tune the *Q* factor over a wide range, while preserving high spatial confinement, may prove useful for applications in which *Q*-factor matching considerations hold [34], such as the development of low-threshold, optically-pumped dye lasers [10].

Acknowledgments

This project was funded by an Army Research Office PECASE Award under Grant 56801-MS-PCS. Computation for work described in this paper was supported by the University of Southern California Center for High-Performance Computing and Communications.

#198966 - $15.00 USD Received 7 Oct 2013; revised 10 Nov 2013; accepted 18 Nov 2013; published 9 Dec 2013